Molecular Microbiology (2019) 0(0), 1–12 doi:10.1111/mmi.14377

Role of flagellar hydrogen bonding in *Salmonella* motility and flagellar polymorphic transition

Chu Wang,[1,2] Michele Lunelli,[1,2] Erik Zschieschang,[2] Jens Bernhard Bosse,[3] Roland Thuenauer[4] and Michael Kolbe[1,2,5]*

[1] *Department of Structural Infection Biology, Center for Structural Systems Biology (CSSB), Helmholtz-Center for Infection Research (HZI), Notkestrasse 85, Hamburg, 22607, Germany.*

[2] *Structural Systems Biology Group, Max Planck Institute for Infection Biology, Berlin, Germany.*

[3] *Department of Structural Cell Biology of Viruses, Subunit Quantitative Virology, Heinrich Pette Institute, Leibniz Institute for Experimental Virology, Hamburg.*

[4] *Advanced Light and Fluorescence Microscopy (ALFM) Facility, Centre for Structural Systems Biology (CSSB), University of Hamburg, Notkestrasse 85, Hamburg, 22607, Germany.*

[5] *MIN-Faculty University Hamburg, Hamburg, Germany.*

Summary

Bacterial flagellar filaments are assembled by tens of thousands flagellin subunits, forming 11 helically arranged protofilaments. Each protofilament can take either of the two bistable forms L-type or R-type, having slightly different conformations and inter-protofilaments interactions. By mixing different ratios of L-type and R-type protofilaments, flagella adopt multiple filament polymorphs and promote bacterial motility. In this study, we investigated the hydrogen bonding networks at the flagellin crystal packing interface in *Salmonella* enterica serovar typhimurium (*S.* typhimurium) by site-directed mutagenesis of each hydrogen bonded residue. We identified three flagellin mutants D108A, N133A and D152A that were non-motile despite their fully assembled flagella. Mutants D108A and D152A trapped their flagellar filament into inflexible right-handed polymorphs, which resemble the previously predicted 3L/8R and 4L/7R helical forms in Calladine's model but have never been reported *in vivo*. Mutant N133A produces floppy flagella that transform flagellar polymorphs in a disordered manner, preventing the formation of flagellar bundles. Further, we found that the hydrogen bonding interactions around these residues are conserved and coupled to flagellin L/R transition. Therefore, we demonstrate that the hydrogen bonding networks formed around flagellin residues D108, N133 and D152 greatly contribute to flagellar bending, flexibility, polymorphisms and bacterial motility.

Accepted 21 August, 2019. *For Correspondence. Email: Michael.kolbe@helmholtz-hzi.de; Tel.: (+49) 40 8998 87500.

Introduction

Salmonella swims by means of flagella, which can turn at a speed of 300 Hz and push cells up to 30 μm/s (DeRosier, 1998). Each *Salmonella* cell possesses 6 to 10 peritrichous flagella with around 10–15 nm in diameter and up to 15 μm in length. The flagellum comprises a basal body, a hook and a filament protruding out from the membrane. The flagellar filament is a tubular supercoiled polymer of approximately 20,000 subunits of a single protein named flagellin. In *S.* typhimurium, flagellin is alternatively expressed as FliC (phase 1 flagellin) or FljB (phase 2 flagellin) (Zieg, *et al.*, 1977; Bonifield and Hughes, 2003). Both flagellin monomers are composed of four connected domains, including highly conserved D0, D1 domains at both the N- and C-terminus, and variable D2 and D3 intervening domains (Wilson and Beveridge, 1993; Yonekura, Maki-Yonekura *et al.*, 2003).

The flagellin subunits are helically arranged along the flagellar filament axis with 11 subunits per two turns (O'Brien and Bennett, 1972). Cutting and unfolding of the tubular lattice formed by flagellin subunits yield a two-dimensional strip of lattice, where subunits are numbered in the order of the filament assembly. Interactions were found at the interfaces of 5-, 6-, 11- and 16-start lattice lines (Yamashita *et al.*, 1998; Yonekura *et al.*, 2003; Friedrich, 2006). The 11 start lines are arranged nearly longitudinal to its axis, and therefore, are named protofilament (O'Brien and Bennett, 1972). According to Calladine's model, each protofilament can switch between two stable states L and R that have different twisting directions and inter-subunit distances (Calladine, 1978; Kamiya

et al., 1979). By assembling different ratios of L- and R-type subunits among the 11 protofilaments, 12 distinct shapes of flagella filaments (polymorphs) have been predicted (Fig. S1), including 10 types of supercoiled and 2 types of straight filaments (Calladine, 1978; Kamiya *et al.*, 1979). The flagellar polymorphs differ in their geometric parameters such as handedness, curvature and twist of the filaments. Various helical forms were identified and classified into left-handed 'normal' (9L/2R), 'coiled' (8L/3R) and right-handed 'semicoiled' (7L/4R), 'curly I' (6L/5R), and 'curly II' (5L/6R) according to their distinct helical pitches and radius (Kamiya *et al.*, 1979; Turner *et al.*, 2000).

Salmonella exhibits an alternate run-and-tumble swimming motion that performs reversible transformations between different polymorphs of flagella (Berg and Brown, 1972). When all the motors rotate counterclockwise (CCW, viewed from distal end of flagellar filament), the flagella adopt 'normal' helical form and assemble into a bundle that generates a thrust force to propel the bacterium forward (Berg and Stryer, 2002). When one or more motors rotate clockwise (CW), the flagellar bundle unwinds, flagella transform in the sequence of semicoiled, curly I and curly II forms leading to cell tumbling (Turner *et al.*, 2000). The switching between running and tumbling mode allows the chemotaxis and thermotaxis behavior of bacteria (Macnab and Ornston, 1977). Besides swimming cells, flagellar polymorphic transformations are also observed when influenced by mechanical forces, point mutations and environmental factors such as pH values and salt concentration (Kamiya and Asakura, 1976; Macnab and Ornston, 1977; Kamiya *et al.*, 1979; Calladine *et al.*, 2013).

In the present study, we analyze the role of conserved hydrogen bonds in flagellar polymorphism and bacterial motility by alanine substitutions of residues involved in inter-molecular interactions of flagellin subunits in *S.* typhimurium. We identify interactions that are essential for bacterial motility even though not impeding the flagellar assembly. We further investigate the flagellar dynamics of three flagellin alanine mutants at residues D108, N133 and D152 and demonstrate their involvements in the protofilament L/R switching, flagella stability and polymorphic transformation.

Results

Inter-subunit interactions in flagellin crystals

We have recently solved the structure of the FljB flagellin of *S.* typhimurium containing domain D1 to D3 (residues 55 to 459) and lacking the D0 domain (J.A. Horstmann, M. Lunelli, unpublished, PDB ID: 6RGV) (Fig. 1A). The crystallized FljB shows conserved D1 domain and similar crystal lattice arrangement to FliC flagellin in *S.* typhimurium, *Bacillus subtilis* (*B. subtilis*) and *Pseudomonas aeruginosa* (*P. aeruginosa*) (Fig. S2A, B) (Samatey *et al.*, 2001; Song and Yoon, 2014; Altegoer *et al.*, 2018).

The interface area between two stacked subunits in the truncated FljB crystal is about 820 Å^2 and comprises

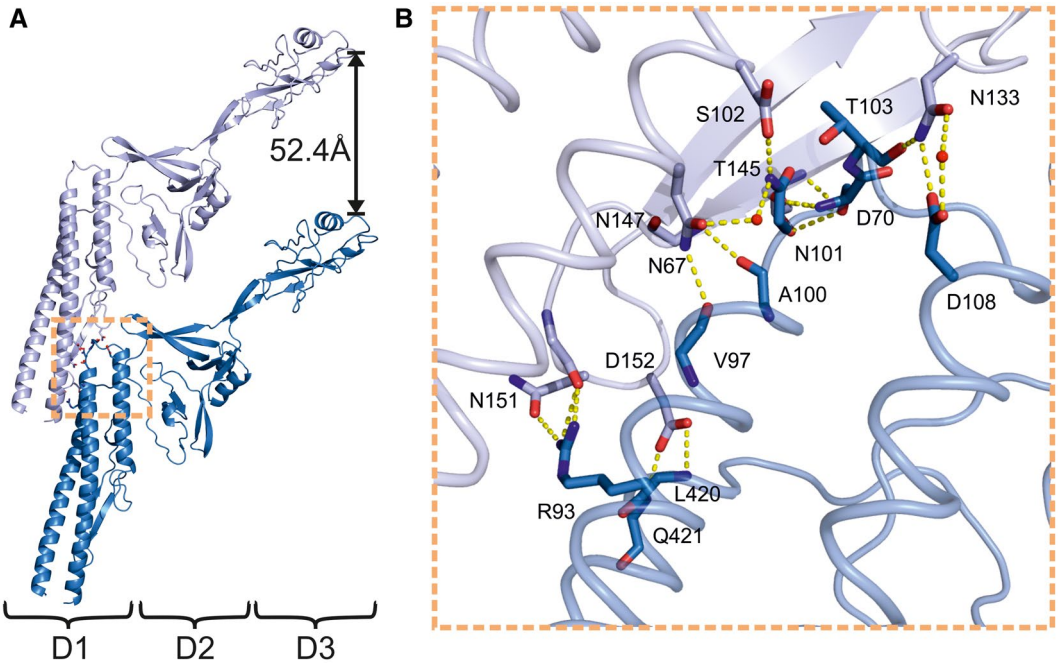

Fig. 1. Atomic detail of inter-subunit interactions of FljB in crystals. A. Arrangement of two stacked FljB subunits in the crystal. The domain D1 forms the backbone from which the domains D2 and D3 protrude. The distance between subunits in the stack is indicated. B. Close-up view of the interactions in boxed region of Fig. 1A. Residues involved in inter-subunits interactions are highlighted as stick model and hydrogen bonds as dashed yellow lines. Red dots represent water molecules.

mainly the D1 domain, formed by a long coiled coil with a shorter helix and a β-hairpin packed against it. In the upper molecule, residues 55-74, 132-135 and 142-155 that belong respectively to the N-terminal α-helix of the coiled coil, the loop and the β-hairpin, contribute to the interface. In the lower subunit, residues 86-108 and 418-427 that belong to the D1 domain coiled coil and to the turn that connects it to the shorter helix interact with the upper subunit. Residues 324-327 that form a β-turn in domain D2 complete the interface of the lower molecule. In total, we found 13 inter-subunit hydrogen bonds and 2 water molecules connecting residues of domain D1 (Fig. 1b, Table 1). Except for hydrogen bonds formed by A100/Q147 and S102/T145, which involve only interactions between the protein backbone, most hydrogen bonds include one (five pairs) or two (six pairs) side chains (Table 1).

Notably, the inter-subunit interfaces and distances between stacked subunits are conserved among different flagellin crystal structures and cryo-EM reconstructions of the flagellar filament (Fig. S2, Table S1), similar inter-subunit distance was also measured by X-ray fiber diffraction in isolated flagellar straight filaments (Table S1) (Yonekura, Maki-Yonekura *et al.*, 2003; Maki-Yonekura, Yonekura *et al.*, 2010). Moreover, we note that two stacked flagellins in crystal structures superpose well with the flagellar cryo-EM structures with root-mean-square deviations of 1.22–1.34 Å for FliC and 1.53–2.57 Å for FljB (Table S2). Therefore, it is reasonable to assume that the truncated flagellin crystal arrangement mimics the flagellar protofilament assembly, as already proposed for the F41 crystals (Samatey *et al.*, 2001). Due to the high resolution in FljB crystal structure (2 Å), which clearly shows the side chains, compared to the flagellar cryo-EM structure (4–8 Å), we decided to use the FljB crystal interface to study the flagellin hydrogen bonding interactions and their role in the flagellar polymorphic transformation.

Table 1. FljB inter-subunit hydrogen bonds

Upper subunit	Lower subunit	Distance (Å)
N67 Nδ	V97 O	3.03
[a]**N67 Oδ**	**N101 Nδ**	3.85
D70 Oδ	**N101 Nδ**	2.95
D70 Oδ	**T103 Oγ**	3.63
N133 Nδ	T103 O	2.82
[a]**N133 Nδ**	**D108 Oδ**	2.85
T145 Oγ	**S102 Oγ**	3.31
T145 O	S102 N	2.90
Q147 N	A100 O	2.93
A150 O	**R93 Nη**	2.91
N151 Oδ	**R93 Nη**	3.29
D152 Oδ	L420 N	3.06
D152 Oδ	Q421 N	2.95

The table lists the residues and atoms involved in the 13 inter-subunit hydrogen bonds found at the interface between stacked FljB subunits as shown in Fig. 1. Distance between the atoms is reported and interactions involving amino acids side chains are bold highlighted.

[a]Water molecules are present between residue pairs N67/N101 and N133/D108.

Flagellar assembly and bacterial swimming behaviors of flagellin mutants

To investigate the relevance of our axial interaction assignment, we generated site-specific *S.* typhimurium mutants in a flagellin knockout (KO) strain carrying plasmid-encoded single alanine mutations in the *fljB* or *fliC* gene (residues highlighted in Table 1 and Fig. S2F). Helical FliC or FljB flagellar filaments protruded from all tested mutant cells without significant differences to those of the wild type as imaged by transmission electron microscopy (TEM) (Fig. S3). These observations indicate that the tested single mutations involved in protofilament inter-subunit interactions have no apparent effect on flagellar assembly (Fig. S3).

Next, we compared the swimming ability of *S.* typhimurium mutants on soft agar plates. Similar results were observed for the corresponding *fljB* and *fliC* mutants. The flagellin mutants bearing single alanine mutations at residues N67, D70, R93, N101, S102, T145 and N151 are still motile, although showed various extents of reduced swimming ability compared to the wild-type flagellin expressing bacteria (Fig. 2A). On the contrary, alanine replacement of residues D108, N133 or D152 resulted in non-motile bacteria (Fig. 2A).

Since the swimming behaviors of corresponding *fljB* and *fliC* mutants were very similar, we focused on the behaviors of the *fljB* mutants for the following studies. To confirm the contribution of the *fljB* mutations to the motility of individual cells, we investigated the swimming trajectories of GFP-labeled FljB mutants S102A, D108A, N133A and D152A in liquid medium. Similar to the movements of wild-type *fljB* expressing cells, the *fljB* S102A mutant showed linear progression and smooth trajectories containing long running phases (Fig. 2B). In contrast, the non-flagellated strain and *fljB* mutants D108A, N133A and D152A displayed chaotic, non-directed trajectories with only small net displacements, which could represent a random walk caused by Brownian motion of the cell body (Fig. 2B). Next, we conducted a mean square displacement (MSD) analysis on the recorded trajectories, where plots of the same strain were averaged (Fig. S4). The diffusion coefficient D and anomalous diffusion exponent α estimated from fits of the respective MSD curves did not reveal notable differences of the diffusional behavior between D108A, N133A, D152A mutants and non-flagellated *S.* typhimurium (Table 2), suggesting that the presence of flagella does not have a noteworthy influence on the bacterial diffusion in liquids. Meanwhile, the D and α values in strains FljB or S102A differed significantly from

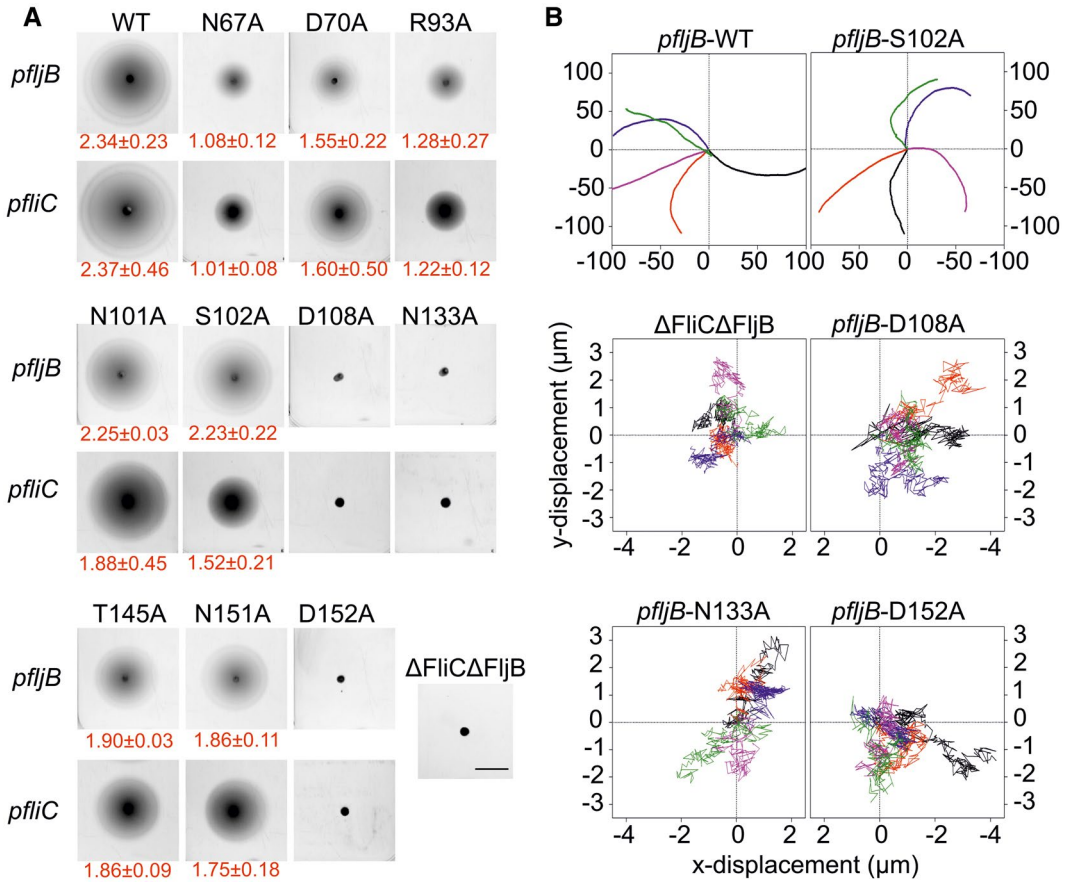

Fig. 2. Characterization of motility phenotypes of *S.* typhimurium *fliC* and *fljB* mutants. Motility of flagellin KO *S.* typhimurium strain (ΔFliCΔFljB) and strains episomally expressing wild-type *fljB*/*fliC* gene (WT) or indicated mutations were tested in swimming plate assays and in liquid culture. A. Bacterial population-based swimming motility was determined using swim agar plates. Averaged migration distances (radius) of three individual measurements are shown below the each swimming halo image. Scale bar is 2 cm. B. Representative trajectories of individual GFP-labeled *S.* typhimurium cells in liquid culture are shown. Each colored line depicts the trajectory of a single bacterium tracked over a duration of 5 s with 40 frames per seconds (fps); the starting point of each trajectory was normalized to 0. Trajectories *pfljB*-WT: $n = 117$; *pfljB*-S102A: $n = 210$; ΔFliCΔFljB: $n = 174$; *pfljB*-D108A: $n = 134$; *pfljB*-N133A: $n = 89$; *pfljB*- D152A: $n = 93$) were analyzed with MATLAB and Icy (Track Manager Plugin) and graphs generated using OriginPro9.

Table 2. Run and tumble motility parameters of individual wild type or mutant *fljB*-expressing bacteria

Mutant	Diffusion coefficient D ($\mu m^2/s$)	Anomalous diffusion exponent α	Tethered cell rotating speed (Hz)	Tethered cell f_{CW}	Fraction of rotating cells (%)
pfljB	167 ± 50	1.94 ± 0.21	1.92 ± 1.19	0.20 ± 0.08	10.00 ± 1.63
pfljB-S102A	150 ± 46	1.93 ± 0.06	1.88 ± 1.15	0.22 ± 0.12	9.80 ± 1.64
pfljB-D108A	0.26 ± 0.13	1.02 ± 0.20	2.07 ± 1.98	0.21 ± 0.08	4.18 ± 0.98
pfljB-N133A	0.24 ± 0.20	0.97 ± 0.14	2.37 ± 1.79	0.19 ± 0.10	10.75 ± 1.5
pfljB-D152A	0.22 ± 0.07	0.92 ± 0.19	2.26 ± 1.38	0.19 ± 0.13	4.83 ± 1.72
ΔFliCΔFljB	0.19 ± 0.06	0.94 ± 0.21	NA	NA	NA

Diffusion coefficient and anomalous diffusion exponent of individual bacteria were estimated from fits of the respective MSD curves in Fig. S4, recording bacteria near surface swimming using fluorescence microscopy (*pfljB*: $n = 58$; *pfljB*-S102: $n = 113$; *pfljB*-D108A: $n = 84$; *pfljB*-N133A: $n = 31$; *pfljB*-D152A: $n = 59$; ΔFliCΔFljB: $n = 85$). Tethered cell rotating speed was averaged by total turns over 30 s (*pfljB*: $n = 77$; *pfljB*-S102: $n = 63$; *pfljB*-D108A: $n = 60$; *pfljB*-N133A: $n = 96$; *pfljB*-D152A: $n = 24$) and the fraction of time spent turning CW (f_{CW} = flagellar CW rotating time spent/total rotating time) (*pfljB*: $n = 73$; *pfljB*-S102: $n = 76$; *pfljB*-D108A: $n = 20$; *pfljB*-N133A: $n = 130$; *pfljB*-D152A: $n = 25$) was calculated from tethered cell rotation data processed by BRAS (Kojadinovic *et al.*, 2011). Fraction of rotating cells is indicated as the percentage of free rotating cells relative to the number of all observed cells. The results were averaged from several observations (*pfljB*: $n = 7$; *pfljB*-S102: $n = 5$; *pfljB*-D108A: $n = 4$; *pfljB*-N133A: $n = 4$; *pfljB*-D152A: $n = 6$) in tethering experiments videos, each field contains 100–200 cells. Data shown represent the mean ± SD. NA: not analyzed.

the other mutants, indicating their active motility behavior and the role of hydrodynamic interactions among flagella and cells.

Altogether, the results of the single cell tracking assay and the swimming plate assay match, indicating that the alanine mutation at flagellin residue D108, N133 or D152 generates non-motile bacteria.

To further elucidate whether these mutations solely abolish the cell's ability to undergo a running motion or whether flagellar rotation is completely abrogated, we investigated the flagellar rotating behavior of individual *S.* typhimurium cells.

Flagellar rotatory motility of FljB mutants

We conducted tethering experiments to determine the flagellar rotating ability and the rotation patterns of different *fljB* mutants. In these assays, individual bacteria were tethered to a glass surface through a single shortened flagellum (Silverman and Simon, 1974), and the motility was visualized through cell body rotation. Properly tethered cells executed stochastic switching between CW and CCW rotations for all tested mutants (Video S1), corresponding to CCW and CW 'run-and-tumble' filament rotations, respectively, when viewed from the distal end of the flagellum. Overall, similar switching patterns were observed for all tested wild-type and mutant FljB strains (Fig. S5). In most cases, flagellum-tethered bacteria rotated dominantly CCW for a few seconds with a stochastically transient CW rotation for deciseconds, which can be interpreted as long 'running' periods interspersed by short 'tumbling' events (Fig. S5A). In rare cases, we also observed cells with continuous 'running' motion that was not interrupted by any 'tumbling' events over 30 s (Fig. S5B), cells with long duration of 'tumbling' events lasting several seconds (Fig. S5C), and cells containing 'pausing' events where the rotation was occasionally stopped and continued in the same direction afterwards (Fig. S5D). Comparable rotation patterns were also found in a previous study with wild-type *E. coli* and *S.* typhimurium (Eisenbach *et al.*, 1990), suggesting that the tested FljB mutants have no defects in the flagellar rotary machinery.

We averaged the cumulative rotating turns over the period of 30 s for individual bacteria as an indicator of overall flagellar rotating speed, in which the CCW rotation was considered as positive and the CW rotation negative. The averaged turns per second varied significantly between individual cells in the same strain, ranging from around 1 Hz up to more than 10 Hz with the major cell portion rotating with a speed between 1 and 5 Hz. These results are in good agreement with previous studies using tethered *Salmonella* strains (Silverman and Simon, 1974; Attmannspacher *et al.*, 2008). When we compared the overall cell rotation speed of different bacterial strains, we found, however, similar speed distribution (Table 2, Fig. 3A) for wild type and the tested mutants ($P > 0.05$). We also calculated the average fraction of time spent turning CW (f_{CW}), and found that cells spent approximately 20 % of the time turning CW among all the tested species with no significant differences (Table 2 and Fig. 3B). This ratio is comparable to the one measured in a previous study using wild-type *E. coli* strain RP437, which spent 0.22 ± 0.05 fraction of the time turning CW (Alon *et al.*, 1998). Altogether, the flagella of *S.* typhimurium non-swimming mutants have similar rotation patterns, speed distributions and tumbling times to that of wild-type *fljB*-expressing bacteria. Therefore, we conclude that the tested flagellar mutations have no apparent effect on flagellar rotation functions.

We observed, however, around 50% less properly tethered or rotating bacteria in *fljB* non-swimming mutants

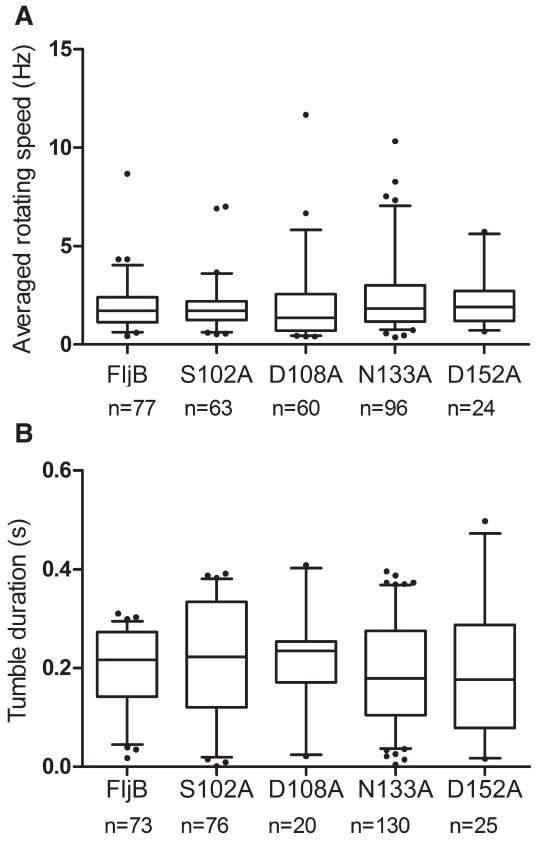

Fig. 3. Rotation assays of surface tethered *S.* typhimurium *fljB* mutants. Single bacteria episomally expressing the *fljB* gene or indicated mutations were tethered to a glass surface. A. Box plot of averaged cell body rotating speeds over 30 s. B. Box plot of fraction of time spent turning CW (f_{CW}) over 30 s. For each box, the lower, middle and upper horizontal lines of the box represent the first quartile, the median and the third quartile respectively. The lower and upper extremities of the lines represent the lowest 5% data and the highest 95% data. The dots represent outliers. Statistical analysis was conducted with one-way ANOVA Gaussian Approximation. $P > 0.05$ was considered as non-significant.

D108A and D152A compared to wild type, D102A and N133A FljB flagellated bacteria (Table 2), suggesting that these two mutations cause the flagella attach less efficiently to the glass surface than the others, probably due to the morphology and surface properties of these filaments.

Dynamic flagellar morphologies and polymorphic transformation

To understand the kinetics of flagellar movement and its impact on bacterial swimming behavior, we monitored flagellar morphologies of near surface free swimming *S.* typhimurium expressing wild type or mutant FljB using live-cell microscopy.

We observed that the flagella of wild type and motile mutant S102A *fljB*-expressing *S.* typhimurium were flexible and elastic while propelling cells forward, and showed classical flagellar polymorphic transitions (videos S2 and S3): In the swimming mode, all flagellar filaments rotated CCW, adopted the 'normal' (9L/2R) waveform and assembled into a helical superbundle that propels a linear smooth motion of bacteria (Fig. 4 frame 1, Videos S2and S3). Occasionally, one (Video S2) or more (Video S3) filaments changed to 'curly II' (5L/6R) waveform, bended and unwrapped from the bundle, while other filaments kept on rotating in a 'normal' waveform as part of the flagellar bundle (Fig. 4 frames 2 to 10). After changing swimming directions, the curly filaments rejoined the bundle and adopted again the 'normal' waveform thus restoring the swimming mode described before (Fig. 4 frames 11 to 20, Videos S2 and S3).

Compared to wild-type FljB, the flagella of the non-swimming mutants D108A and D152A showed different phenotypes, their mutated flagella became very stiff and lost their ability to stretch, bend or transit to any of the above described polymorphs despite of the observed rotatory motion (Video S4 and S5). Flagella of the mutants D108A and D152A were apparently locked in specific waveforms. We measured the pitch and radius of the filaments using the software Fiji (Schindelin *et al.*, 2012) and distinguished the helical handedness as described before (Shimada *et al.*, 1975). FljB mutant D108A has a right-handed waveform with helical pitch of 0.81 ± 0.02 μm and a radius of 0.04 ± 0.01 μm (Table 3, Fig. 5A). The filaments of D152A have a slightly larger right-handed helical pitch of 1.05 ± 0.04 μm and radius of 0.07 ± 0.01 μm (Table 3, Fig. 5B). Our measurements agree well with the calculation of Darnton and Berg (Darnton and Berg, 2007), suggesting that the pitch and radius visualized in mutants D108A and D152A corresponded to the Calladine model of types 3L/8R and 4L/7R respectively (Table 3 and Fig. S1). To our knowledge, these helical forms were hitherto only predicted but never observed in bacterial species *in vi*vo. Comparable pitch and radius of D152A flagella were detected *in vitro* when flagellins from 'normal' and straight flagella were copolymerized with the ratio of 1:9 (pitch 1.05 μm, radius 0.075 μm) (Asakura and Iino, 1972). Noteworthy, we observed the same flagellar helical forms in bacteria producing FliC D108A and D152A mutants, sharing comparable helical pitch and radius (Fig. 5C, 5, Table 3 and Videos S6 and S7). This result indicates that the effects of D108A and D152A mutations are conserved among different types of flagellin.

In the non-swimming FljB mutant N133A, however, the flagella seemed to be more flexible than those of the

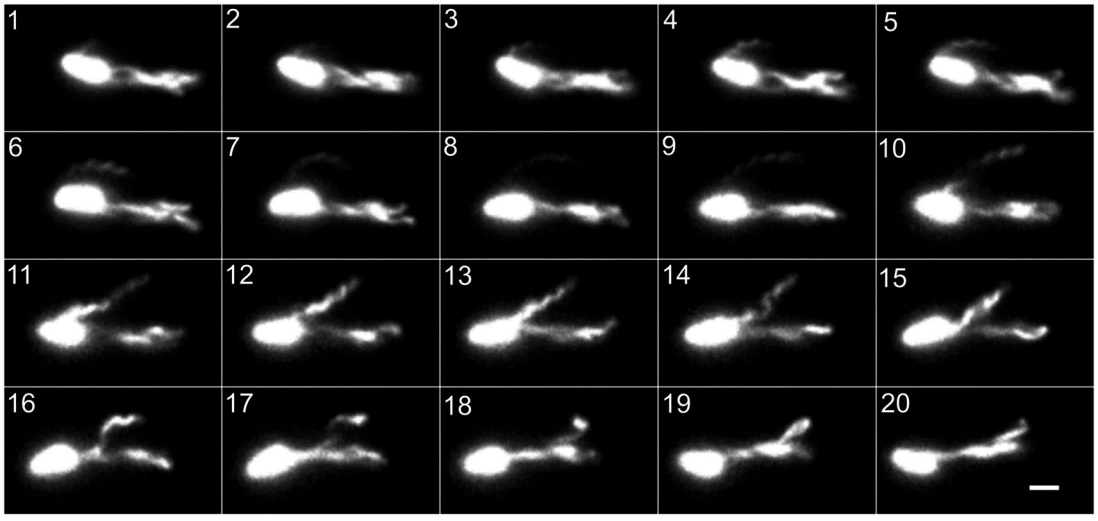

Fig. 4. Flagellar polymorphic transformations of *fljB*-flagellated *S.* typhimurium. Flagellar polymorphic transformations between two 'tumbling' events of flagellar KO *S.* typhimurium episomally expressing *fljB* gene were captured with successive frames at 150 fps. Scale bar is 2 μm. See also the corresponding Supplementary videos S2.

Table 3. Pitch and radius of *Salmonella* flagellar filament helixes

Helical forms	Theory[a]		Measurements in this study[b]			
	Flagellin (μm)		FljB (μm)		FliC (μm)	
	Pitch	Radius	Pitch[c]	Radius	Pitch	Radius
3L/8R (D108A)	0.82	0.03	0.81 ± 0.02	0.04 ± 0.01	0.82 ± 0.07	0.04 ± 0.00
4L/7R (D152A)	0.97	0.06	1.05 ± 0.04	0.07 ± 0.01	0.95 ± 0.06	0.06 ± 0.01
9L/2R (normal)	2.16	0.21	2.17 ± 0.11	0.22 ± 0.01	–	–

[a]Theoretical calculations based on reference (Darnton and Berg, 2007).
[b]For each pitch and radius 20 flagellar filaments were averaged.
[c]Data were shown as Mean ± SD.

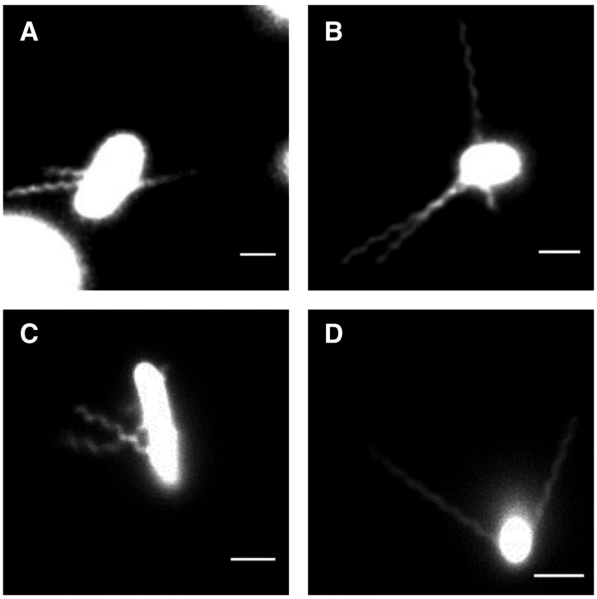

Fig. 5. Flagellar morphologies of flagellin mutants D108A and D152A. Images of the dynamic filament shapes from free swimming *S.* typhimurium episomally expressing *fljB* D108A (A) and D152A (B) or expressing *fliC* D108A (C) and D152A (D). The flagella in mutant D108A and D152A are locked to right-handed helical forms 3L/8R and 4L/7R respectively. Scale bar is 2 μm. See also the corresponding Supplementary Video S4–S7.

wild-type cells, adopting a mixture of several polymorphs simultaneously. Their flagella underwent unsynchronized polymorphic transformations and bending during the measurements, and running/tumbling motions could not be clearly differentiated. Consequently, the N133A mutant was unable to form a flagellar bundle and performed a chaotic scrambled vibration at one spot instead of a linear swimming trajectory (Fig. 6, Videos S8 and S9).

In summary, the residues D108, N133 and D152 that form the hydrogen bonds at flagellar protofilament subunit interfaces critically determine flagellar polymorphic transformations, flagellar bundle formation and bacterial motility.

Discussion

Flagella polymorphic transformation allows bacteria to swim toward or away from attractive or repellent signals. Despite many intensive and advanced studies in flagellar fiber diffraction (Yamashita *et al.*, 1998), crystallography (Samatey *et al.*, 2001), cryo-EM (Yonekura *et al.*, 2003; Maki-Yonekura *et al.*, 2010; Wang *et al.*, 2017) and computational simulations (Kitao *et al.*, 2006) deciphering the details of the flagellar structure and function, the mechanisms of flagellar supercoiling and flagellar polymorphic transition are still not fully understood. We noticed that the truncated flagellin stacks found in crystals mimics flagellar protofilament assembly with conserved inter-subunit interfaces and repeat distances among bacteria flagellum containing 11 protofilaments (Tables S1, S2 and Fig. S2). In fact, as reported previously, the major part of flagellin termini is not essential for forming filaments in vitro, and flagellins with large truncation of terminal region could still assemble into filaments in the presence of wild-type flagellin seeds (Mimori-Kiyosue *et al.*, 1996). The high-resolution crystal structure of flagellin allowed us to identify the hydrogen bonds at the subunit interfaces and analyze their impact on the bacterial motility. We first found the presence of a redundant network of interactions formed between subunits by observing that single mutation of the hydrogen bonded residues in FljB or FliC flagellins still grow helical flagella *in vivo*. While most of the mutated flagella caused a reduced swimming ability of *S.* typhimurium, mutants D108A, N133A and D152A lost their swimming ability completely despite flagellar rotating motions. We showed that hydrogen bond breakage by alanine mutation at D108 or D152 aborts flagellar polymorphic transformation ability and favors the formation of the right-handed helix flagella with dominant R-type protofilaments. On the contrary, the previously reported mutation D108E strengthens the polar contact and leads to L-type straight filaments (Kanto *et al.*, 1991; Hayashi *et al.*, 2013). The mutant N133A, different

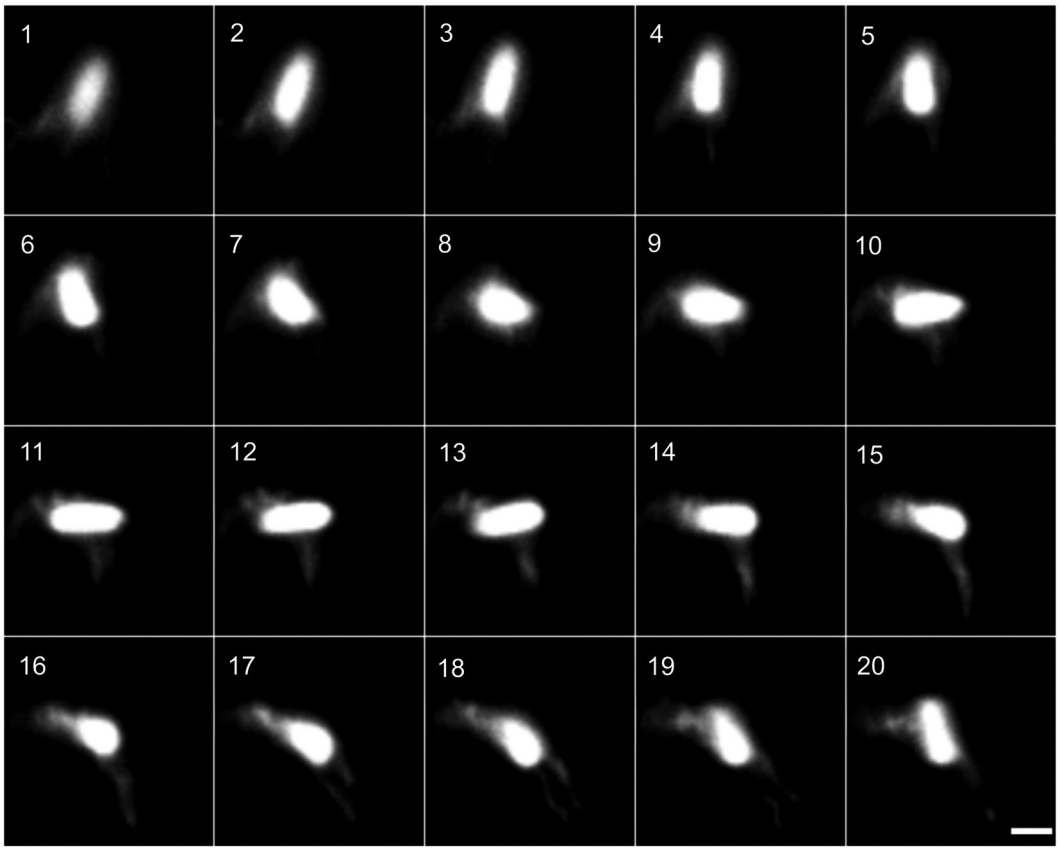

Fig. 6. Representative flagellar polymorphs of FljB mutant N133A. The flagellar movements of flagella KO *S.* typhimurium episomally expressing *fljB* gene carring N133A mutation were captured with a successive frame rate of 150 fps. Mixed helical forms of flagellar filaments are shown in each frame. The flagellar filaments underwent unsynchronized polymorphic transformations and no bundle formation was observed. Scale bar is 2 μm. See also the corresponding Supplementary Videos S8 and S9.

from D108A and D152A, formed floppy and disordered flagella that were unable to transform between different waveforms in an organized manner and, consequently, not forming a flagellar bundle. Taken together, this indicates that the hydrogen bonds between flagellin subunits are not only controlling the static curvature and twist of flagellar filaments, but are also important for keeping organized flagellar polymorphic transformation when propagating the motor thrust. It is worth to mention that we were able to capture for the first time two extreme right-handed helical forms *in vivo* that fit well to the Calladine's model 8R/3L and 7R/4L (Fig. S1), and with the help of high speed microscopy we observed detailed disordered flagellar movements.

The bi-stable protofilament packing and flagellar polymorphic transformations are therefore sensitive to specific amino acids and interactions. Indeed, as reported previously, multiple point mutations have been identified to form straight flagellar filament (Kanto *et al.*, 1991; Hayashi *et al.*, 2013). By applying second-site mutations on straight flagella filaments, several residues have been found to generate functional flagella and recover the swimming ability of bacteria (Wang *et al.*, 2012; Hayashi *et al.*, 2013). Wang *et al* have found that mutations that stabilize flagella in coil or 'curly I, II' forms, were motile due to the fact that they can deform into the 'normal' helical form through rotation, whereas straight filament cannot (Wang *et al.*, 2012). Similar results were obtained in force-biased molecular dynamics simulations, where the transformable helical forms of flagellar filaments were mostly identified in the range from 2R/9L to 6R/5L states upon torque application (Kitao *et al.*, 2006). In comparison, the helical forms 8R/3L and 7R/4L produced by mutants D108A and D152A, respectively, are beyond this range and unable to transform, presumably because they formed more stable right-handed helices with smaller helical pitches and radius (Fig. S1). Our assumption agrees with the study of Kuhn *et al*, which proved that smaller diameter and pitch of flagellar helix stabilize the flagellar filaments (Kuhn *et al.*, 2018).

In intact flagellar filament, subunit interactions are found between 5-, 6-, 11- and 16-start interfaces and key residues might behave as 'switches' that trigger the different interactions during flagellar polymorphic transformation

(Kitao *et al*., 2006). To understand the contribution of the mutations identified in our study on flagella intra- and inter-protofilament interactions, we mapped the interactions around residues D108, N133 and D152 in flagellar L- and R-types straight filaments using the recently published cryo-EM model of *P. aeruginosa* and *B. subtilis*, which share conserved D0/D1 inner core with *S.* typhimurium (Wang *et al*., 2017). Interestingly, although the protein sequences and subunit arrangements are slightly different between crystalized FljB fragment and cryo-EM flagellar structure of *P. aeruginosa* and *B. subtilis*, the local interactions near the residues D108, N133 and D152 are similar (Figs. S1F and S6). Comparing the L- and R-types straight filaments packing in *P. aeruginosa* and *B. subtilis*, there is a clear shift of the hydrogen bonding network coupled to flagellar protofilaments L/ R transition especially along 5-, 11- and 16-start filament interfaces. In *P. aeruginosa* L-type straight filaments, hydrogen bonds are formed between D108 and Q49 at 16-start interface and between T131 and R53 at 5-start interface (Fig. S6B); while in its R-type straight filaments, the same D108 forms hydrogen bond with R53 at 16-start interface and the same T131 interacts with Q57 and N152 at 5-start interface (Fig. S6C). In *B. subtilis* L-type filaments, hydrogen bonds are formed between K51 and N133, N162 and E131 at 5-start interface (Fig. S6E); while in its R-type filaments, the same K51 forms hydrogen bond with D108 at 16-start interface, Q55 forms hydrogen bonds with G134 and the N162 and E131 forms multiple hydrogen bonds with Q165 and R129 (Fig. S6F). These observations strongly suggest that the hydrogen bonds transitions around D108, N133 and D152 are critical for the subunits displacements. We also noticed that the R-type conformation has more interactions at this area than the L-type, contributing to the shortening of R-type protofilament as reported previously (Maki-Yonekura *et al*., 2010).

We therefore conclude that, the residues D108, N133 and D152 characterized in this study play important roles in the flagellar assembly, stability and protofilament L/R switching interactions. We believe that our study provides new insights into the flagellar dynamics at the molecular level.

Experimental procedures

Bacterial cloning and cultivation conditions

The genes *fljB* or *fliC* were amplified from *S.* typhimurium strain SL1344 following standard PCR protocols using primers with BsaI restriction sites. PCR products were cloned into the expression vector pASK-IBA3plus (IBA GmbH). Single alanine point mutations at residue N67, D70, R93, N101, S102, D108, N133, T145, N151 and D152 in p*fljB* or p*fliC* were generated respectively, using QuikChange Site-Directed Mutagenesis Kit (Stratagene). All constructs were confirmed by DNA sequencing. The constructs were expressed in the non-flagellated strain EM812 (SL1344 Δ*fliC* Δ*fljB*) kindly provided by Prof. Marc Erhardt (Humboldt Universität zu Berlin, Germany).

Bacteria were grown in lysogeny broth (LB) supplemented with ampicillin (100 µg/ml) at 37 °C. Bacterial growth was measured using optical density at 600 nm in a Varioskan Flash plate reader (Thermo Fisher Scientific). Target gene expression was induced with anhydrotetracycline hydrochloride (AHT); the concentration of AHT was optimized based on the bacteria swimming ability on swim soft agar plate.

Swimming plate assay

Bacteria inoculated from overnight culture were grown in LB media at 37°C; protein production was induced with 16.67 ng/ml AHT for 2 h. In the swimming plate assay, 2 µl of normalized subcultures with OD_{600} equal to 1.5 were spotted on a center of a plate containing 0.25% LB agar (w/v) and further incubated for 8–10 h at 37°C.

Bacterial TEM imaging

Bacteria were fixed with 2% of paraformaldehyde for 1 h at room temperature (RT). After fixation, cells were rinsed two times with water and stored at 4°C. For electron microscopy, cells were adsorbed to carbon coated copper grids (Electron Microscopy Sciences), washed with distilled water and negatively stained with 4% of phosphotungstic acid for 30 s. Specimens were examined with a Zeiss Leo 906E transmission electron microscope (Carl Zeiss AG).

Single cell tracking in liquid culture

Live imaging was conducted with bacteria expressing the fluorescent protein TagGFP2 (Subach *et al*., 2008) to facilitate single-cell tracking. Bacteria expressing *fljB* single-point mutations were grown until OD_{600} ~ 1.0 in LB medium at 37°C. GFP and FljB productions were induced with 25 ng/ml AHT for 2 h. Cells were diluted 1:300 in fresh LB medium, transferred to an ibidi microcopy chamber and observed at 20°C with a Leica TCS SP8 microscope (20× objective) (Leica Microsystem). About 10–50 individual *fljB*-expressing bacteria were tracked simultaneously using 2D live cell fluorescence microscopy (Ex: 488 nm, Em: 500–520 nm). Image series were recorded for 35 s with 40 frames per second (fps) and trajectories spanning at least 5 s were extracted and subsequently analyzed by the Spot Tracking and Track Manager plug-ins of the Icy image analysis platform (Chenouard *et al*., 2013). A mean squared displacement analysis (MSD) of the bacterial trajectories was performed using the MATLAB class @msdanalyzer (Tarantino *et al*., 2014). MSD curves were derived from the spatiotemporal data of each track and plots belonging to the same flagellin construct were averaged. Fitting was performed by modeling the MSD curves with a power law to account for anomalous diffusion. Fits with $R^2 > 0.95$ were considered for the calculation of the diffusion coefficient and anomalous diffusion exponent from the fitting parameter. The Mann–Whitney U-test was used to determine statistical significance of the mean values.

Tethered cell assay

Bacteria inoculated from overnight culture were grown at 37°C till OD_{600} ~ 0.3 and protein production was induced with 16.67 ng/ml AHT for 2 h. Cells from 1 ml culture were harvested by centrifugation at 1200 g for 5 min, washed three times with motility buffer (0.01 M K_3PO_4, 0.067 M NaCl, 0.1 mM EDTA, pH 7.0), re-suspended in motility buffer supplemented with 50 mM of glycerol and 1 μM of L-Methionine and passed through a 27-gauge needle 36 times to shear off the flagella. A 10 μl drop of the suspension was loaded into a tunnel slide spaced with two layers of sticky tapes as previously described (Silverman and Simon, 1974). The cells were allowed to attach to the coverslip for 15 min at RT and unattached cells were washed away with tether buffer. Cells were visualized at dark field using a Leica TCS SP8 confocal laser scanning microscope with a 63× objective. Videos of stably rotating bacteria were selected and recorded at 40 fps for 30 s. Imaging analysis was conducted using Fiji (Schindelin *et al*., 2012) and modified BRAS (Bacterial Rotation Analysis Software, Open Source Software) (Kojadinovic *et al*., 2011). Statistical analysis was performed with GraphPad Prism 5.0 (GraphPad Software, Inc.). Differences between groups were considered to be significant at a P value of < 0.05 using one-way ANOVA and Gaussian Approximation.

Observation of flagellar filaments

Bacteria were grown and collected as described above. Cells were re-suspended in motility buffer and stained with 0.4 mg/ml cyanine 3 monosuccinimidyl ester (Cy3, Ex: 555 nm, Em: 565 nm, AAT bioquest Inc.) for 1 h at RT as described previously (Turner *et al*., 2000; Scharf, 2002). Sodium bicarbonate (40 mM) was added to maintain pH around 8.0. To remove excess dye, the sample was washed three times by centrifugation with replacement of the supernatant with fresh motility buffer. The final suspension of fluorescently labeled bacteria was diluted around 20-fold in motility buffer supplemented with 0.05% of Tween 20 (w/v) and 0.1 M of glucose. A 2 μl drop of the suspension was carefully loaded onto a humid blue square chamber spaced with silicones to form a layer about 50 μm between the bottom of the chamber and coverslip. Samples were evaluated immediately at RT for a time period not longer than 2 h. FljB flagellated cells were observed using an inverted TiE microscope (Nikon Corporation) with a 100 × 1.49 NA oil immersion objective in oblique illumination mode using objective-TIRF illuminator and laser illumination with a Cy3 Quad filterset (Semrock). Images were acquired using a cropped Andor 897 EM-CCD camera turned to high frame rates through hardware triggering. FliC flagellated cells were observed with a DMi8 inverted wide field microscope (Leica) with a 100 × 1.4 NA oil immersion objective, a Lumencor SOLA SE FISH 365 LED light source and a Cy3 filter cube. Images were acquired using a Leica DFC9000 GT camera (with ROI cropping). Videos of swimming cells were taken for 1 min and image analysis was conducted with Fiji (Schindelin *et al*., 2012). For each helical form, radius and pitch of the flagella helix were measured from static frames in which the flagellum was clear and parallel to the focal plane.

Mapping interaction sites on flagellin subunits

PDB files for illustrating neighboring FljB subunits were generated in our laboratory (J.A. Horstmann, M. Lunelli, unpublished). The atomic model of flagellin fragment F41 (accession no. 1IO1) (Samatey *et al*., 2001), the reconstitution maps for L- and R-types flagellin (accession no. 5wk6 and 5wk5) from *Pseudomonas aeruginosa* (Wang *et al*., 2017) were retrieved from the Protein Data Bank. Residues localization and interaction analysis were performed using the molecular graphics PyMOL and 'Protein interfaces, surfaces and assemblies' service PISA at the European Bioinformatics Institute (http://www.ebi.ac.uk/pdbe/prot_int/pistart.html) (Krissinel and Henrick, 2007).

Acknowledgements

We would like to thank Marc Erhardt for providing the strain EM812, Keiichi Namba for providing the *Salmonella* flagella protein coordinates, Ulrike Abu-Abed and Christian Goosmann for help with electron microscopy images, Jutta Lambers for lab technical support, Imke Spoering, Claudia Trasak and Martin Aepfelbacher for help with samples preparation of time-lapse microscopy and Juana de Diego for her helpful discussions in preparing the manuscript. This work was funded by the European Research Council under the European Community's Seventh Framework Program (FP7/2007–2013, 311374) and the Helmholtz Association funding agency IVF (Initiative and Networking Fund) to Michael Kolbe. The Heinrich Pette Institute, Leibniz Institute for Experimental Virology is supported by the Freie und Hansestadt Hamburg and the Bundesministerium für Gesundheit (BMG).

Author contributions

M.K., C.W. and M.L. conceived and designed the research. C.W., M.L., E.Z., J.B. and R.T. performed the experiments. C.W. and M.K. wrote the manuscript.

Conflict of interest

The authors declare that they have no conflicts of interest in connection with the content of this article.

References

Alon, U., Camarena, L., Surette, M.G.y Arcas, B.A., Liu, Y., Leibler, S. and Stock, J.B. (1998) Response regulator output in bacterial chemotaxis. *EMBO Journal*, **17**(15), 4238–4248.

Altegoer, F., Mukherjee, S., Steinchen, W., Bedrunka, P., Linne, U., Kearns, D.B. and Bange, G. (2018) FliS/flagellin/FliW heterotrimer couples type III secretion and flagellin homeostasis. *Scientific Reports*, **8**(1), 11552.

Asakura, S. and Iino, T. (1972) Polymorphism of Salmonella flagella as investigated by means of in vitro

copolymerization of flagellins derived from various strains. *Journal of Molecular Biology*, **64**(1), 251–268.
Attmannspacher, U., Scharf, B.E. and Harshey, R.M. (2008) FliL is essential for swarming: motor rotation in absence of FliL fractures the flagellar rod in swarmer cells of *Salmonella* enterica. *Molecular Microbiology*, **68**(2), 328–341.
Berg, H.C. and Brown, D.A. (1972) Chemotaxis in Escherichia coli analysed by three-dimensional tracking. *Nature*, **239**(5374), 500–504.
Berg, J.M., Tymoczko, J.L. and Stryer, L. (2002) *Biochemistry*. 5th edition. Section 34.4, A Rotary Motor Drives Bacterial Motion. New York: W H Freeman.
Bonifield, H.R. and Hughes, K.T. (2003) Flagellar phase variation in Salmonella enterica is mediated by a posttranscriptional control mechanism. *Journal of Bacteriology*, **185**(12), 3567–3574.
Calladine, C.R. (1978) Change of waveform in bacterial flagella – role of mechanics at molecular level. *Journal of Molecular Biology*, **118**(4), 457–479.
Calladine, C.R., Luisi, B.F. and Pratap, J.V. (2013) A "mechanistic" explanation of the multiple helical forms adopted by bacterial flagellar filaments. *Journal of Molecular Biology*, **425**(5), 914–928.
Chenouard, N., Bloch, I. and Olivo-Marin, J.C. (2013) Multiple hypothesis tracking for cluttered biological image sequences. *IEEE Transactions on Pattern Analysis and Machine Intelligence*, **35**(11), 2736–3750.
Darnton, N.C. and Berg, H.C. (2007) Force-extension measurements on bacterial flagella: triggering polymorphic transformations. *Biophysical Journal*, **92**(6), 2230–2236.
DeRosier, D.J. (1998) The turn of the screw: the bacterial flagellar motor. *Cell*, **93**(1), 17–20.
Eisenbach, M., Wolf, A., Welch, M., Caplan, S.R., Lapidus, I.R., Macnab, R.M., et al. (1990) Pausing, switching and speed fluctuation of the bacterial flagellar motor and their relation to motility and chemotaxis. *Journal of Molecular Biology*, **211**(3), 551–563.
Friedrich, B. (2006) A mesoscopic model for helical bacterial flagella. *Journal of Mathematical Biology*, **53**(1), 162–178.
Hayashi, F., Tomaru, H., Furukawa, E., Ikeda, K., Fukano, H. and Oosawa, K. (2013) Key amino acid residues involved in the transitions of L- to R-type protofilaments of the *Salmonella* flagellar filament. *Journal of Bacteriology*, **195**(16), 3503–3513.
Kamiya, R. and Asakura, S. (1976) Helical transformations of Salmonella flagella in vitro. *Journal of Molecular Biology*, **106**(1), 167–186.
Kamiya, R., Asakura, S., Wakabayashi, K. and Namba, K. (1979) Transition of bacterial flagella from helical to straight forms with different subunit arrangements. *Journal of Molecular Biology*, **131**(4), 725–742.
Kanto, S., Okino, H., Aizawa, S. and Yamaguchi, S. (1991) Amino acids responsible for flagellar shape are distributed in terminal regions of flagellin. *Journal of Molecular Biology*, **219**(3), 471–480.
Kitao, A., Yonekura, K., Maki-Yonekura, S., Samatey, F.A., Imada, K., Namba, K. and Go, N. (2006) Switch interactions control energy frustration and multiple flagellar filament structures. *Proceedings of the National Academy of Sciences*, **103**(13), 4894–4899.
Kojadinovic, M., Sirinelli, A., Wadhams, G.H. and Armitage, J.P. (2011) New motion analysis system for characterization of the chemosensory response kinetics of Rhodobacter sphaeroides under different growth conditions. *Applied and Environment Microbiology*, **77**(12), 4082–4088.
Krissinel, E. and Henrick, K. (2007) Inference of macromolecular assemblies from crystalline state. *Journal of Molecular Biology*, **372**(3), 774–797.
Kuhn, M.J., Schmidt, F.K., Farthing, N.E., Rossmann, F.M., Helm, B., Wilson, L.G., et al. (2018) Spatial arrangement of several flagellins within bacterial flagella improves motility in different environments. *Nature Communications*, **9**(1), 5369.
Macnab, R.M. and Ornston, M.K. (1977) Normal-to-curly flagellar transitions and their role in bacterial tumbling. Stabilization of an alternative quaternary structure by mechanical force. *Journal of Molecular Biology*, **112**(1), 1–30.
Maki-Yonekura, S., Yonekura, K. and Namba, K. (2010) Conformational change of flagellin for polymorphic supercoiling of the flagellar filament. *Nature Structural & Molecular Biology*, **17**(4), 417–422.
Mimori-Kiyosue, Y., Vonderviszt, F., Yamashita, I., Fujiyoshi, Y. and Namba, K. (1996) Direct interaction of flagellin termini essential for polymorphic ability of flagellar filament. *Proceedings of the National Academy of Sciences*, **93**(26), 15108–15113.
O'Brien, E.J. and Bennett, P.M. (1972) Structure of straight flagella from a mutant *Salmonella*. *Journal of Molecular Biology*, **70**(1), 133–152.
Samatey, F.A., Imada, K., Nagashima, S., Vonderviszt, F., Kumasaka, T., Yamamoto, M. and Namba, K. (2001) Structure of the bacterial flagellar protofilament and implications for a switch for supercoiling. *Nature*, **410**(6826), 331–337.
Scharf, B. (2002) Real-time imaging of fluorescent flagellar filaments of Rhizobium lupini H13–3: flagellar rotation and pH-induced polymorphic transitions. *Journal of Bacteriology*, **184**(21), 5979–5986.
Schindelin, J., Arganda-Carreras, I., Frise, E., Kaynig, V., Longair, M., Pietzsch, T., et al. (2012) Fiji: an open-source platform for biological-image analysis. *Nature Methods*, **9**(7), 676–682.
Shimada, K., Kamiya, R. and Asakura, S. (1975) Left-handed to right-handed helix conversion in Salmonella flagella. *Nature*, **254**(5498), 332–334.
Silverman, M. and Simon, M. (1974) Flagellar rotation and the mechanism of bacterial motility. *Nature*, **249**(452), 73–74.
Song, W.S. and Yoon, S.I. (2014) Crystal structure of FliC flagellin from Pseudomonas aeruginosa and its implication in TLR5 binding and formation of the flagellar filament. *Biochemical and Biophysical Research Communications*, **444**(2), 109–115.
Subach, O.M., Gundorov, I.S., Yoshimura, M., Subach, F.V., Zhang, J., Gruenwald, D., et al. (2008) Conversion of red fluorescent protein into a bright blue probe. *Chemistry & Biology*, **15**(10), 1116–1124.
Tarantino, N., Tinevez, J.Y., Crowell, E.F., Boisson, B., Henriques, R., Mhlanga, M., et al. (2014) TNF and IL-1 exhibit distinct ubiquitin requirements for inducing NEMO-IKK

supramolecular structures. *Journal of Cell Biology*, **204**(2), 231–245.
Turner, L., Ryu, W.S. and Berg, H.C. (2000) Real-time imaging of fluorescent flagellar filaments. *Journal of Bacteriology*, **182**(10), 2793–2801.
Wang, W., Jiang, Z., Westermann, M. and Ping, L. (2012) Three mutations in Escherichia coli that generate transformable functional flagella. *Journal of Bacteriology*, **194**(21), 5856–5863.
Wang, F., Burrage, A.M., Postel, S., Clark, R.E., Orlova, A., Sundberg, E.J., et al. (2017) A structural model of flagellar filament switching across multiple bacterial species. *Nature Communications*, **8**(1), 960.
Wilson, D.R. and Beveridge, T.J. (1993) Bacterial flagellar filaments and their component flagellins. *Canadian Journal of Microbiology*, **39**(5), 451–472.
Yamashita, I., Hasegawa, K., Suzuki, H., Vonderviszt, F., Mimori-Kiyosue, Y. and Namba, K. (1998) Structure and switching of bacterial flagellar filaments studied by X-ray fiber diffraction. *Natural Structural Biology*, **5**(2), 125–132.
Yonekura, K., Maki-Yonekura, S. and Namba, K. (2003) Complete atomic model of the bacterial flagellar filament by electron cryomicroscopy. *Nature*, **424**(6949), 643–650.
Zieg, J., Silverman, M., Hilmen, M. and Simon, M. (1977) Recombinational switch for gene expression. *Science*, **196**(4286), 170–172.

Supporting Information

Additional supporting information may be found online in the Supporting Information section at the end of the article